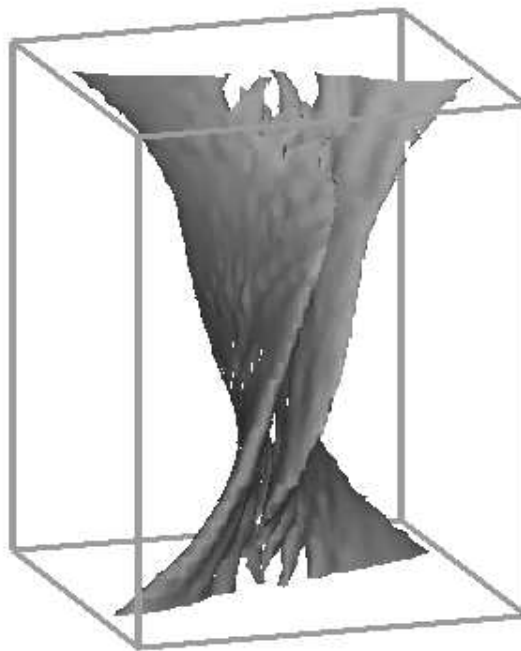
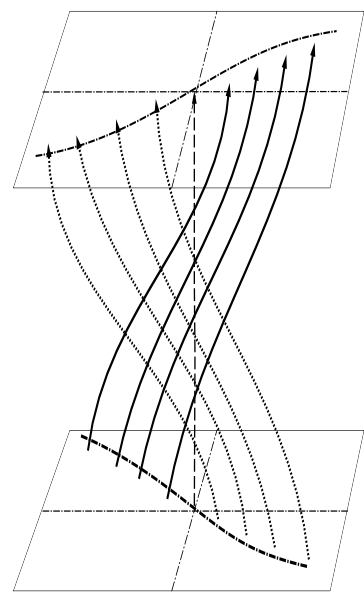
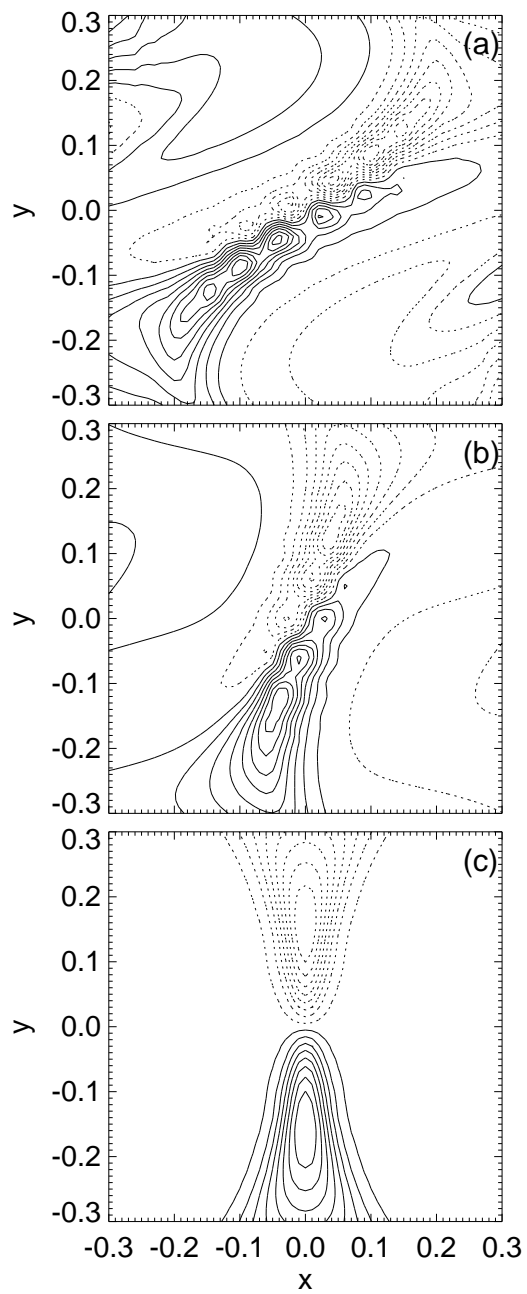


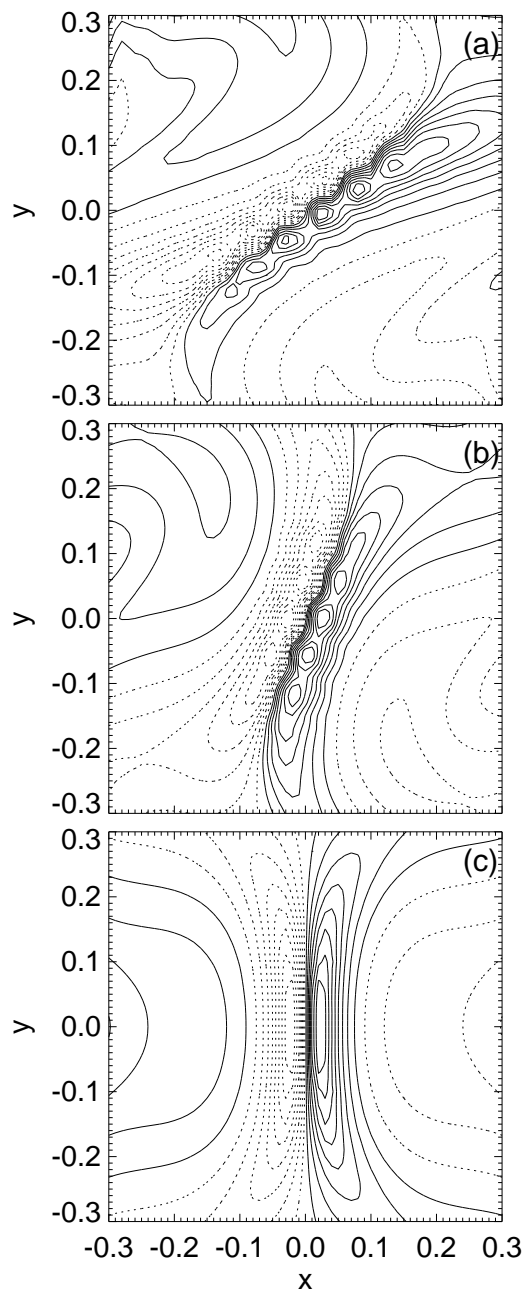
(a)

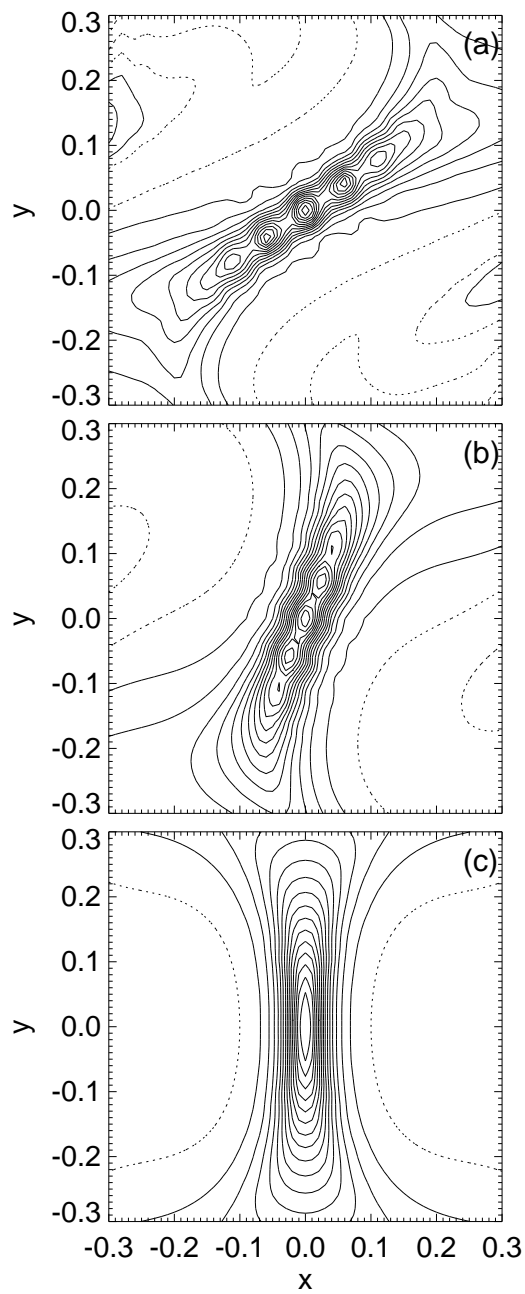


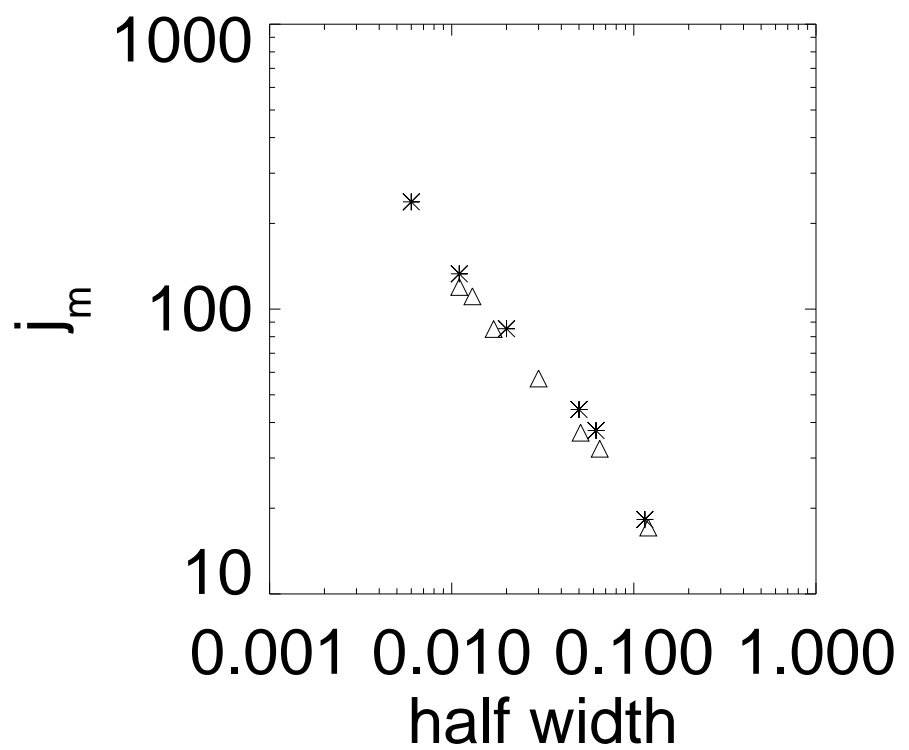
(b)

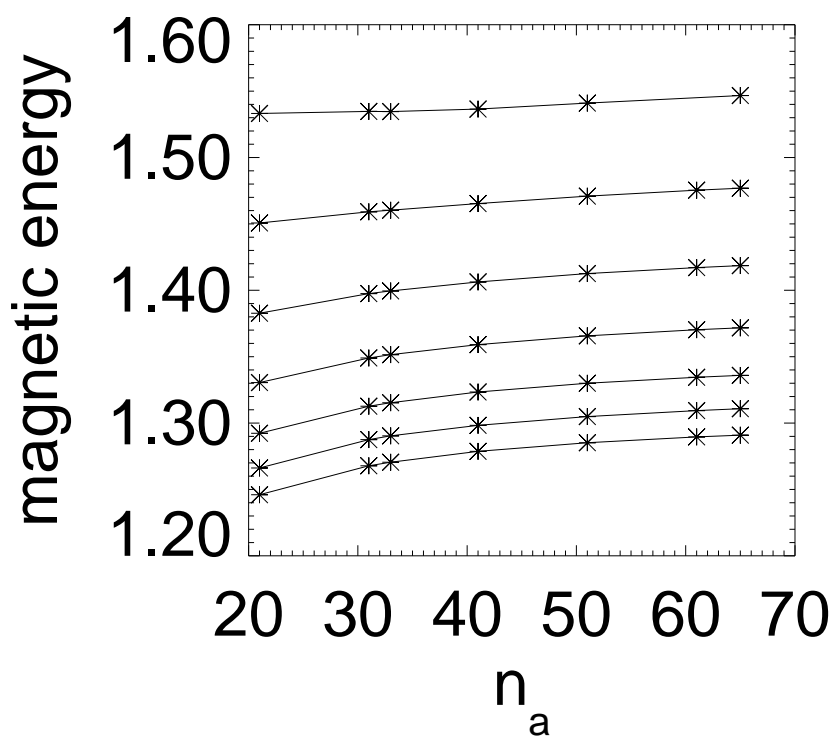
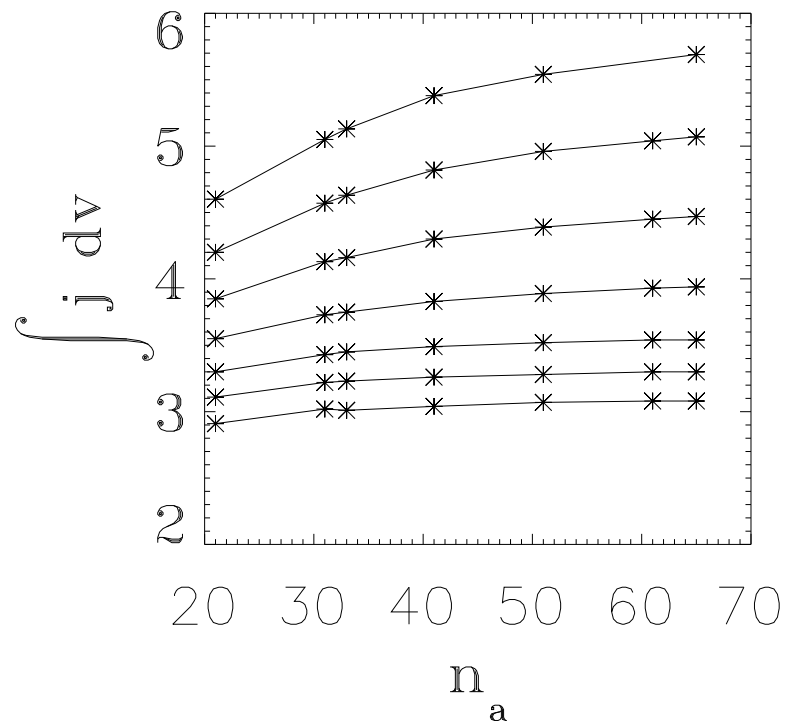


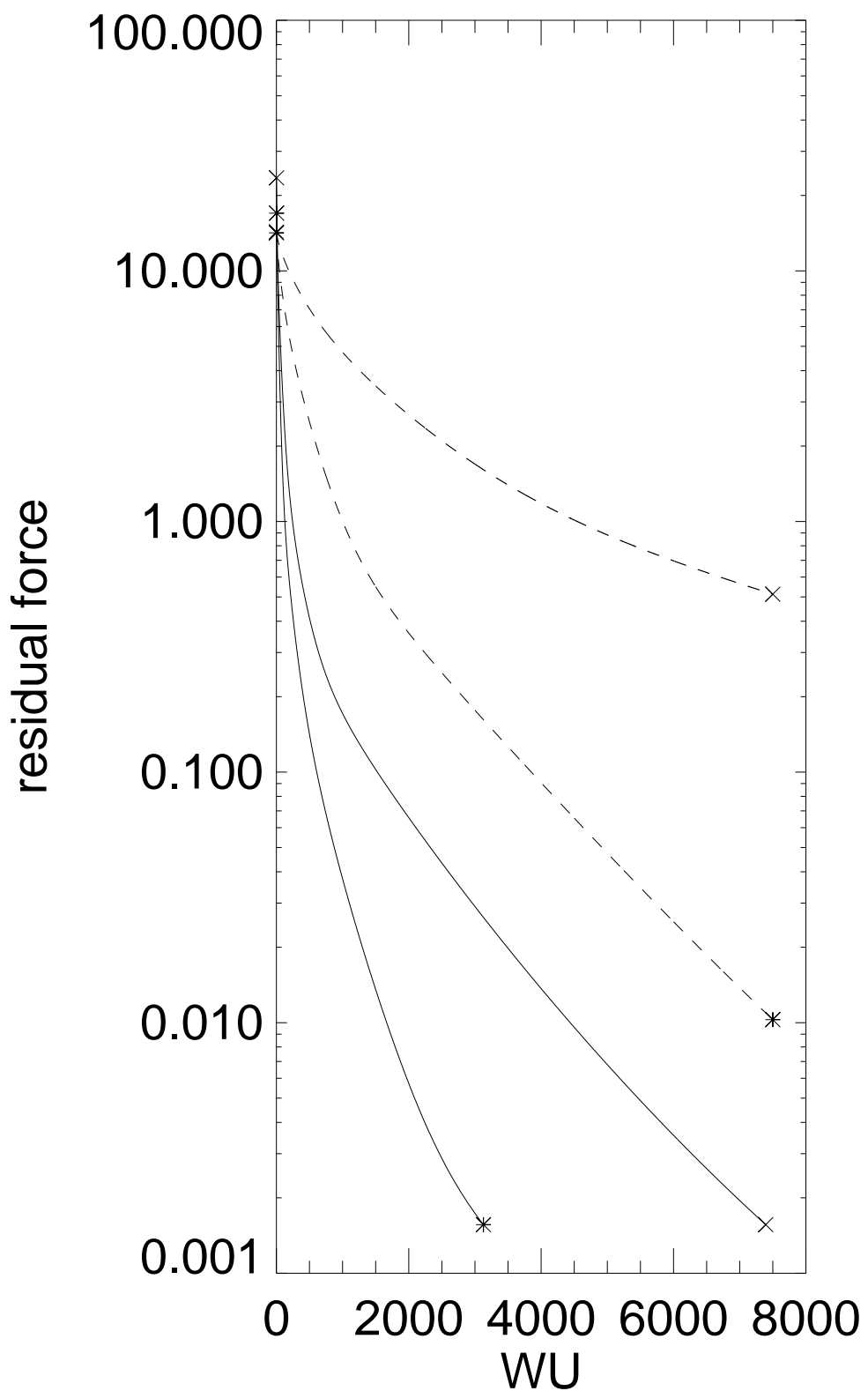


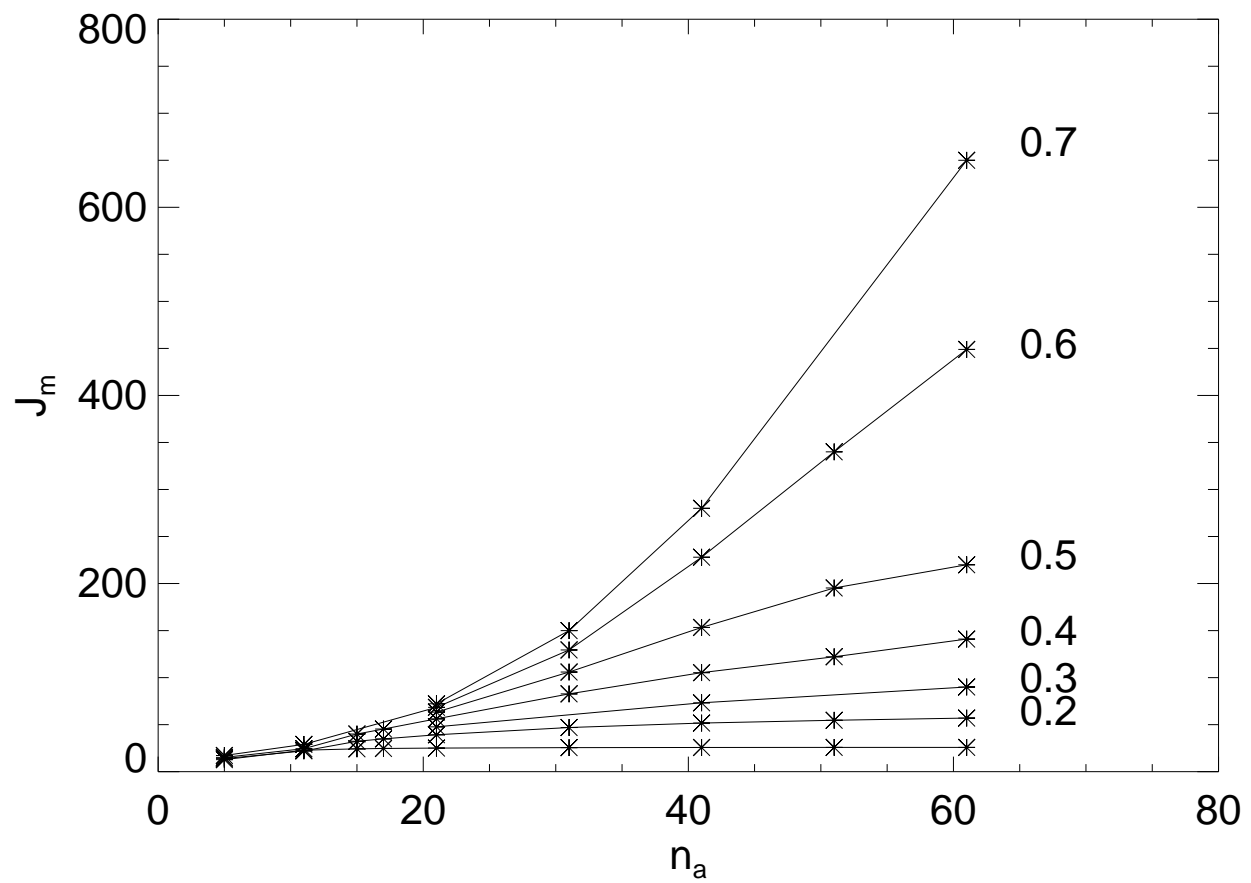












Magnetic Flux Braiding: Force-Free Equilibria and Current Sheets

A. W. Longbottom and G. J. Rickard¹

*Dept. of Mathematical and Computational Sciences,
University of St. Andrews, KY16 9SS, Scotland.*

and

I. J. D. Craig and A. D. Sneyd

Dept. of Mathematics, Waikato University, Hamilton, New Zealand.

ABSTRACT

We use a numerical nonlinear multigrid magnetic relaxation technique to investigate the generation of current sheets in three-dimensional magnetic flux braiding experiments. We are able to catalogue the relaxed nonlinear force-free equilibria resulting from the application of deformations to an initially undisturbed region of plasma containing a uniform, vertical magnetic field. The deformations are manifested by imposing motions on the bounding planes to which the magnetic field is anchored. Once imposed the new distribution of magnetic footpoints are then taken to be fixed, so that the rest of the plasma must then relax to a new equilibrium configuration. For the class of footpoint motions we have examined, we find that singular and nonsingular equilibria can be generated. By singular we mean that within the limits imposed by numerical resolution we find that there is no convergence to a well-defined equilibrium as the number of grid points in the numerical domain is increased. These singular equilibria contain current "sheets" of ever-increasing current intensity and decreasing width; they occur when the footpoint motions exceed a certain threshold, and must include both twist and shear to be effective. On the basis of these results we contend that flux braiding will indeed result in significant current generation. We discuss the implications of our results for coronal heating.

Subject headings: MHD, Solar Corona, Current Sheets, Coronal Heating, Flux Braiding

¹present address: The Met Office, London Road, Bracknell, Berks, RG12 2SZ, UK

1. Introduction

Accounting for the elevated temperature of the corona is a fundamental issue in solar observation and theory. For many it is the magnetic field that is at the heart of the mystery, acting as the link between the convective motions in the photosphere and the resultant currents and resistive dissipation in the corona itself. Such a link was perhaps first developed by Gold (1964), and subsequently formalised to some degree by Parker (1972,1983) in his notion of “topological dissipation” to describe the process by which twisting and braiding of the ambient magnetic field can lead to energy release in the corona. Indeed, in his 1972 paper, Parker reduced the problem to that of considering nothing more than a uniform field contained between a pair of superconducting plates. This latter configuration has become known as “Parker’s model”, and has proved useful as a testing ground for coronal heating theories.

The currents j produced in the corona must be of significant intensity to account for coronal heating. This is because the coronal resistivity η (typically of the order of $10^{-12} \text{Mm}^2\text{s}^{-1}$) in the ohmic dissipation term ηj^2 is so small that only currents of a sufficient magnitude can lead to energy deposition within the required coronal timescales. To produce such currents, the magnetic field must be able to collapse to sufficiently small scalelengths. Indeed, if we take the equilibrium field to contain scalelengths of order unity, then we require a collapse by at least six orders of magnitude to generate the intense currents. Such fine scale current structures we shall refer to as “current concentrations”. These are to be contrasted with “current sheets” which are taken to be those structures resulting from spatial discontinuities in the magnetic field direction, and whose existence within the framework of ideal magnetohydrodynamics (MHD) is generally considered to be singular, in that it is only the presence of finite resistivity that allows their spatial extent to be resolved. Current concentrations, on the other hand, can be resolved within ideal MHD. However we choose to define these features, it is this vast range of scalelengths they imply that certainly makes the task of finding evidence for them so challenging.

From an analytical point of view, Parker’s model (1972) contends that current sheets will in general be created in coronal magnetic fields. This is based on Parker’s belief that equilibrium is only possible if an

ignorable coordinate exists in the magnetic field perturbations. Given the random nature of photospheric flows, it seems unlikely that the perturbations will possess a certain symmetry. Therefore, in order to proceed towards an equilibrium, the magnetic field must regain this symmetry, and to do so the field must alter its topology. Parker suggests that this is accomplished through current sheets and magnetic reconnection. Since the topology is changed through the nonidealness of the plasma, the term “topological dissipation” was coined. However, van Ballegooijen (1985, 1988a) has pointed out a flaw in Parker’s original analysis, and claims in his own right that the field can pass through a series of equilibria without requiring reconnection. These equilibria are continuous and have no symmetry. Hence it is the time evolution through these equilibria that can lead to coronal heating via current concentrations, and not as a result of the coronal field attempting to relax to any particular equilibrium state. The jury is still out on this issue, however, as evidenced by Parker’s recent work (1994).

Numerical attacks have been made on the problem, notably van Ballegooijen (1988b, 1990), Mikić et al (1989), Longcope and Sudan (1994), Galsgaard and Nordlund (1996) and Hendrix and Van Hoven (1996). On the evidence from such modelling it does seem plausible that magnetic scalelengths much smaller than those proscribed for the imposed flows can result in the corona, thereby lending weight to this process being a coronal heating mechanism. Furthermore, the work of Mikić et al (1989) shows that force-free equilibria without current sheets can be generated for each particular distribution of footpoints comprising the overall evolution. Longcope and Strauss (1994a,b) have examined the formation of current layers with a nonzero, but small, thickness. They show, through the analysis of the Jacobian of the fieldline mapping, that these current concentrations may easily be more than six orders of magnitude smaller than the equilibrium length scale. The resulting structures they observe bear a marked resemblance to those we find in this paper, albeit through the use of different methods to those presented here. On the basis of these few experiments it would seem that the weight of evidence is against Parker. However, as we have previously noted, the coronal scalelengths actually envisaged are so small as to be out of the reach of such numerical simulations for the foreseeable future. We must therefore tread carefully in extrapolating the

numerical results to actual coronal conditions.

In order to try to alleviate the numerical shortfall, resulting from the severe scalelength constraints, Craig and Sneyd (1986) (1990) developed a magnetic relaxation technique using a Lagrangian scheme. Such a scheme permits the numerical mesh to move with the fluid elements and magnetic field lines comprising the plasma. Consequently, as any short scalelengths develop in a region of the plasma, so the Lagrangian scheme will aggregate more grid points there. This means that for the same number of initial numerical nodes as an Eulerian code might have, the Lagrangian scheme will be able to resolve much finer scales. This is clearly an advantage when the search is directed specifically towards finding evidence of current concentrations or sheets. We will therefore be using the Lagrangian scheme in this study. This is not to say that the Lagrangian code is a panacea for all our resolution ills, since we still need to have sufficient resolution over the whole magnetic structure containing any of these current structures. Even allowing for this latter constraint, there is no doubting the efficacy of the Lagrangian scheme in allowing us to explore a greater range of parameter space than would be accessible to any Eulerian code for the equivalent amount of computing power.

We wish, therefore, to directly test Parker's model of current sheet formation using the Lagrangian relaxation scheme. The method allows us to find the nonlinear, force-free equilibria consistent with the imposed magnetic footpoint displacements. We are consequently only interested in the final magnetic configuration within the constraints of ideal MHD. This contrasts with most of the previous numerical studies of this problem which were Eulerian and time-dependent. It should be noted, however, that although in the absence of definitive analytic and numerical diagnostics, we cannot be certain that a solution with a singular current sheet is necessarily the end result of a given numerical experiment, our results at least indicate those configurations with the potential to develop field singularities.

The layout of the paper is as follows. In Section 2 we outline the basic equations and method of solution, and detail the numerical experiments that we have undertaken. Section 3 presents the results and analysis from these experiments, and we finish with a discussion and some conclusions in Section 4.

2. Model and Numerical Details

2.1. Basic Equations

For this particular study we adopt the low- β approximation for the solar corona and look for equilibrium solutions of the equation,

$$(\nabla \times \mathbf{B}) \times \mathbf{B} = 0, \quad (1)$$

where \mathbf{B} is the magnetic field. These equations are nonlinear. To find solutions of these equations we follow the relaxation method detailed by Craig and Sneyd (1986) (1990) and use a momentum equation which ignores inertial effects in favour of a dominant frictional term proportional to the fluid velocity \mathbf{v} , and takes gas pressure to be negligible in line with the low- β approximation. This simply leaves us with,

$$\mathbf{v} = \mathbf{j} \times \mathbf{B}, \quad (2)$$

where the current $\mathbf{j} = \nabla \times \mathbf{B}$. In this form the momentum equation guarantees relaxation toward a state of lower magnetic energy. The equation set is completed by noting that \mathbf{B}/ρ satisfies,

$$\frac{D}{Dt} \frac{\mathbf{B}}{\rho} = \left(\frac{\mathbf{B}}{\rho} \cdot \nabla \right) \mathbf{v}, \quad (3)$$

where ρ is the fluid density, D/Dt is the so-called convective derivative, and

$$\nabla \cdot \mathbf{B} = 0. \quad (4)$$

The details for the solution of these equations using Lagrangian coordinates can be found in Craig and Sneyd (1986) (1990). The vital step is the realisation that the whole problem can be formulated in terms of the Lagrangian position of a fluid element \mathbf{x} , say, by replacing \mathbf{v} by $D\mathbf{x}/Dt$, and using the so-called Cauchy solution for equation (3) which expresses \mathbf{B}/ρ in terms of the equilibrium magnetic field \mathbf{B}_0 , density ρ_0 , and \mathbf{x} itself. The resultant system of equations is parabolic, as shown by Craig and Sneyd (1990). As a consequence, unconditionally stable numerical schemes must be used to solve the system if inefficiently small time steps are to be avoided. The implicit formulation devised by Craig and Sneyd (1986) gives the requisite numerical stability, and can be solved using alternating direction implicit (ADI) techniques. It should be noted that although Lagrangian, the equations themselves are solved on a fixed grid using centered differences.

As for all classical methods, the number of iterations required for convergence scales as some power of the number of points (N) in the system, typically as N^2 . Thus for numerical schemes in three dimensions, doubling the size of the computational domain requires approximately 64 times the number of iterations. It was found that for this simulation grids of over 32^3 required an excessively long computational time. In order to somewhat alleviate this problem we have implemented a nonlinear multigrid algorithm for grid sizes of 32^3 or more. For such a scheme the number of iterations scale at a fraction of that of classical methods thus allowing high resolution calculations to be conducted in realistic times. Our method is outlined in the appendix.

2.2. The Numerical Experiments

Our equilibrium configuration is exactly that envisaged by Parker (1972), i.e., a uniform, vertical magnetic field $\mathbf{B}_0 = B_0\hat{\mathbf{z}}$, with its ends anchored into superconducting plates at $z = \pm L_z$. The initial positions of the fluid elements are distributed uniformly throughout a domain bounded by the superconducting plates in z , and by distances $x = \pm L_x$ and $y = \pm L_y$. In the previous experiment of the nonlinear evolution of the kink instability detailed by Craig and Sneyd (1990), the fluid elements lying in the bounding planes in x and y were taken to be fixed. Therefore only fluid elements inside the computational domain were free to move. In our initial experiments we adopted the same boundary conditions. However, the nature of our experiments meant that we generated boundary layers at the x and y bounding planes which tended to mask the physics of importance. To overcome this problem, the x and y directions are taken to be periodic in the displacements of the fluid elements, leaving the only fluid elements fixed to be those in the planes $z = \pm L_z$. Apart from the initial equilibrium, this is the only major change to the classical Lagrangian code from its previous incarnation under Craig and Sneyd (1990). However for the systems with large shears and large numbers of grid points a nonlinear multigrid scheme has also been implemented (see Longbottom, Fielder and Rickard (1997) for further details).

Starting from the equilibrium distribution just detailed, we impose displacements of the fluid elements within the planes $z = \pm L_z$. These displacements take the form of shears of equal magnitude but opposite direction on the two driving boundaries. Once dis-

placed, these elements are then held fixed, and the remaining fluid elements are allowed to relax towards a new equilibrium configuration consistent with these new boundary conditions. We say that we have a converged solution when both our norm of the residual force has fallen to at least $O(10^{-3})$ (starting at $O(10)$) and the maximum current has converged to two decimal places. By solving the ideal MHD equations, we guarantee that the magnetic field lines are “frozen-in” to the fluid. The equilibrium field lines in this case are vertical lines running from the bottom to the top boundary in z , so that fluid elements initially sharing the same values of x and y lie on the same field line. As we have intimated, they will lie on the same field line throughout the relaxation. We can therefore plot any relaxed field line simply by drawing a line through that same set of fluid elements. This results from our choice of equilibrium, and using the Lagrangian coordinate system.

For every single solution, we attempt to detail numerical convergence in the solution by repeating the same relaxation with ever increasing numbers of fluid elements. In this way we hope to separate out equilibria that are non-singular (smooth) from those that are singular, i.e., containing current sheets. If the equilibrium is singular, then increasing the numbers of fluid elements will not result in a convergent maximum current in the current sheet. The scalelength of such a singular feature will always be smaller than that attainable numerically, and so the current locally will continue to increase. However, the total current in the computational domain will converge, showing that the global solution is convergent, apart from the locality of the singularity. On the other hand, the nonsingular solutions will converge to a smoothly resolved structure throughout the whole domain. Even with the Lagrangian code, the ultimate lack of numerical resolution means that the convergence properties of any equilibrium solution are all that we can base our physical results upon. The relaxation experiments described by Billingham et al (1993) to examine current sheet formation in two-dimensional fields provide a substantive example of this process, and it is indeed their convergence tests that we have employed here. It should be noted that although increasing the number of grid points reduces the numerical error for a particular solution, the solution itself depends on the position of the Lagrangian grid points. Within the confines of one dimensional theory it can be shown that the motion of the Lagrangian

grid allows a better representation of the true solution as compared to an Eulerian grid with the equivalent number of grid points. The maximum current that may be resolved scales as the square of the number of grid points. The behaviour in a higher number of dimensions is not so obvious, but for many cases an improved representation of the true solution over the equivalent Eulerian code is found.

Having outlined the basis for our numerical experiments, we now need to consider possible footpoint motions. The key ingredient is to produce scalelength collapse of the magnetic field within the volume as a result of smooth displacements on the boundary. This is the crux of Parker's model (1972). Clearly, fine scale motion on the boundary will manifest itself as fine scales within the volume. However, the observations suggest that the scale of convective motion in the photosphere is much greater than we envisage for the current sheets. It must therefore be left up to the coronal magnetic field to produce the short scalelengths of its own accord. Parker (1972) believed that the coronal magnetic field always does, and hence the notion of topological dissipation.

Our particular choice of footpoint motions are motivated by the work of Galsgaard and Nordlund (1996). They conclude that the most important factor leading to current sheet formation is one shear in one direction followed by another in the orthogonal direction. This process is deemed to be sufficient to produce the exponential current growth predicted by van Ballegooijen (1986) on the basis of a random series of shearing motions. As Galsgaard and Nordlund (1996) note, it is the underlying field and flow topology resulting from the shear plus a shear that inevitably leads to the exponential growth. It seems clear that the alternating shear flow profiles advocated by van Ballegooijen (1988a), and tested by van Ballegooijen (1988b) and Mikić et al (1989), will still lead to the exponential growth, since the sequence of footpoint motions is indeed composed entirely of the basic element, i.e., a shear plus a shear. To simplify the problem as much as possible, then, we choose to examine the possible effect on the coronal field of a shear in one direction, followed by a shear in the same, or in another, direction. It is these basic elements that we are going to focus on here.

In the numerical experiments, distances are normalised to the initial length of each field line, and we take the normalising magnetic field strength and plasma density to be those in the equilibrium. For

the experiments we have conducted to date, we use the unit cube as the initial volume of our numerical domain, and we take the field strength to be one and density to be 0.05. These provide the reference points when we later detail results from the relaxed equilibria.

To maximise the spatial resolution available to us, we will simply examine the equilibria associated with the footpoint displacements shown in Figures A1(a)-(f). Figure A1(a) shows the initial equilibrium footpoints. At every grid point (at the intersection of grid lines) lies the footpoint of each magnetic field line. The Lagrangian code follows these particular points, so that after each successive distortion of the grid we can exactly identify where the original footpoint locations shown in Figure A1(a) have been moved to. Figure A1(b) results from a shear of magnitude 0.8 applied parallel to the y -axis. The remaining Figures A1(c)-(f) result from shears of magnitudes 0.1, 0.3, 0.5, and 0.7, respectively, applied parallel to the x -axis *after* having previously applied the shear resulting in Figure A1(b). We are therefore examining the effect of shearing in one direction, immediately followed by shearing in the perpendicular direction. We hope to show that this is sufficient to produce scalelength collapse within the plasma volume. It should be noted that the displacements on the boundaries $L = \pm L_z$ are of the same magnitude but of opposite sign.

From the evidence of some of the gross grid distortions shown in the previous Figures, the reader may be surprised that we can claim to obtain relaxed equilibria from such complex arrangements. We should point out, however, that we have shown the physical grid displacements, and not the uniform grid on which the resulting Lagrangian equations are actually solved. As we shall show, the more distorted the system, the more difficult the relaxed equilibrium is to obtain. Nevertheless, given sufficiently robust relaxation techniques, the Lagrangian system should allow us to approach the equilibrium associated with each set of footpoints arbitrarily closely.

Although we have detailed the footpoints, there is still the question about what to use as the starting points for the fluid elements within the computational volume. As Craig and Sneyd (1990) have intimated, we have a nonlinear equation to solve, and it is therefore possible that differing initial conditions for the same footpoint distribution will result in different relaxed states. While it would be interesting to

explore this hypothesis, we are faced with the more practical problem of obtaining any relaxed equilibria at all. This is because not all initial conditions lead to solutions, despite the unconditional numerical stability of the Lagrangian code. It seems that sometimes the code finds an initial condition too complex to be able to sensibly unscramble, and fails. The best strategy we have found to date is to use as an initial guess the relaxed solution from the previous state in the sequence of footpoint displacements, with the new footpoint displacements prescribed on the boundaries $z = \pm L_z$. So, although we view each equilibrium as an entirely separate solution to all the others, there is a sense in which they can be viewed as a sequence connected together. The “dynamical” experiment of Mikić et al (1989) falls into this category.

Having applied the footpoint displacements to the end planes at $z = \pm L_z$, these are then held fixed, and the remaining fluid elements are able to move in such a way as to approach a new equilibrium consistent with the footpoint distribution. How close we are to the new equilibrium is measured by the maximum Lorentz force $\mathbf{j} \times \mathbf{B}$ within the domain. Having obtained a “suitably good” solution, we then calculate the maximum current within the domain, and the total integrated current strength $|\mathbf{j}|$ over the whole domain. We then repeat the whole experiment for increasing numbers of fluid elements within the domain. The whole exercise is then repeated for each new distribution of footpoints. Based on these results, we are then in a position to comment on the smoothness or otherwise of a given equilibrium solution.

Our ability to catalogue each equilibrium accurately is limited firstly by the available computing power, and secondly (and perhaps more importantly) by the speed at which the equilibrium solution is approached numerically. The last feature is compounded by increasing numbers of fluid elements and the increasing complexity of each equilibrium solution. This means that, even with the implementation of multigrid techniques, the equilibria associated with the most distorted grids are not only the hardest to solve computationally, but also, because of their inherent problems, are the ones on which we have the least amount of numerical convergence.

3. Results

The summary of all our results is encapsulated in Figure A2. This plots the maximum absolute value

of the current J_m obtained within the computational domain (always at the centre of the mid-plane in z) in the best relaxed solution, against a measure of the number of grid points in the simulation n_a . Here the total number of points in the simulation is equal to n_a^3 , and the measure of the best relaxed solution is that with the lowest maximum value of the Lorentz force $\mathbf{j} \times \mathbf{B}$ obtained so far. The number labelling each curve shows the amplitude of the shear applied in the x -direction, while the unlabelled curve refers to that in Figure A1(b). Converged solutions (either using the classical relaxation method or nonlinear multigrid) are plotted with an $*$, those that are under estimates of the current are plotted with a Δ .

Figure A2 reveals that j_m is tending to saturate for the lower set of shears applied, i.e., up to and including 0.5. We would therefore conclude that these reveal smooth equilibria. However, for the shears labelled by 0.6 and 0.7 the value of J_m is tending to increase at least linearly with n_a , so that within the confines of our resolution we would conclude that these point to the possibility of (at least) significant current concentrations, if not current sheets themselves. It should be noted that, within the confines of a one dimensional Lagrangian representation, a rigorous condition for a truly singular current sheet may be obtained. This states that the maximum current J_m must scale as n_a^2 . If this is taken as a generally necessary condition for current sheet formation, then only equilibria with a shear of 0.7 exhibit singular behaviour, J_m scaling approximately linearly with n_a for a shear of 0.6. It is not however obvious how the effect of working in a higher number of dimensions would modify the condition. Thus we refer to both shears of 0.6 and 0.7 as divergent solutions.

Although we have a broad range of footpoint distributions, the generic forms of the relaxed solutions we see divide themselves into two types, at least with respect to the structure of the current. The first is associated with shearing only in the y -direction. Here there is no specific peaking of the current distribution. Rather we have a relatively broad current structure filling most of the domain. As Figure A2 shows, we require only relatively modest numbers of fluid elements before we confidently predict that the equilibrium is a convergent one with respect to n_a . Indeed, for certain parameters, this equilibrium may be calculated analytically (Hood, priv. comm.). For these cases the numerical method reproduces the true solution to within the given tolerance. The basic field structure

as a function of x of these solutions is shown in Figure A3. Figure A3(a) shows the variation of B_x with the height z . The bold curve with the largest amplitude is B_x close to the lower z boundary. As you go up in z the amplitude of B_x gradually falls, resulting in the second bold curve plotted at about half way between the lower z boundary and the mid-plane. In the mid-plane, B_x is zero. From the mid-plane upwards the variation in B_x is a mirror image of that below the mid-plane, with the sign of B_x reversed (as indicated by the dashed curves). There is only a single curve shown for B_y in Figure A3(b) as the relaxed B_y is practically uniform in z . The variation in B_z is similar to that for B_x , i.e., a weak boundary layer at the top and the bottom, with hardly any z -variation about the mid-plane. The only difference is that there is no sign change in B_z , hence the two curves, the larger amplitude one in the mid-plane, and the other close to the z -boundaries.

We also note that the variation in x of B_y exactly matches of that of the imposed footpoint displacement, i.e., proportional to $\sin(2\pi x)$, whereas B_z has half the wavelength. This variation in B_z results from the need to balance the excess magnetic pressure in the y -direction produced by the footpoint shear. B_z therefore has to match the x -gradient of B_y^2 , resulting in the x -profile we see. To produce this B_z profile the fluid elements have to displace themselves in the x -direction in order to generate regions of either increased or decreased B_z . Since our fluid elements are tied to the field lines, this x -motion naturally results in a B_x that has the same wavelength as B_z , but is $\pi/2$ out of phase.

These first type of solutions are therefore almost wholly dependent on x alone about the mid-plane, with most of the variation in z occurring towards the top and bottom planes. The lowest energy state for our boundary conditions seems to be one in which an almost one-dimensional structure extends over most of the domain, with most of the stress taken up in the weak boundary layers. This is reminiscent of results reported by Browning and Hood (1989) and references therein in the context of twisted flux tubes in which, as here, the equilibrium is practically one-dimensional everywhere, except for boundary layers near the line-tied boundaries. This seems to be the lowest energy configuration with respect to one in which, as might have been anticipated, there is a gradual variation in the properties of the equilibrium over the whole length of the structure.

The second (and most important) type of current structure is revealed in all the other relaxed solutions, once a second shear in the x direction has been applied. The only thing that distinguishes each of these particular solutions is the amplitude of the current obtained. Each solution contains a strong current concentration restricted to a narrow slice passing through the centre of each z -plane, which then rotates slowly as increasingly higher z -planes are passed through. The amplitude of the maximum current in each plane in this feature is practically constant along its length, peaking in the central plane at $z = 0$, and diminishing only very gradually towards the two ends. The main component of the current is in the z -direction. A representation of this feature is shown in Figure A4, which shows the isosurface at 50 per cent of the maximum current in j_z . Larger amplitudes of j_z are enclosed within this isosurface, and this surface therefore reveals the extent of the current concentration (and consequently its halfwidth, that we define later). The effect of the shear is apparent in the twist of the structure. We also note that there is just a single isosurface at this level in the volume.

Representative isosurfaces in the same relaxed solution for the currents j_x and j_y are shown in Figure A5(a) and Figure A5(b), respectively. Comparing with Figure A4 we see that the isosurfaces for j_x and j_y exhibit the same twist, but that instead of a single isosurface we now see the presence of two isosurfaces that, to a first approximation, tend to wholly enclose the 50 per cent isosurface for j_z . In common with j_z , however, j_y shows a fairly uniform spatial distribution in z , whereas j_x has a broader distribution near the bounding planes in z , which then narrows and rotates as the mid-plane is approached from either side.

The explanation for the second type of current structure is fairly simple, and has been detailed by Galsgaard and Nordlund (1996). It all boils down to how the field lines wrap themselves around one another as a result of the two sets of shears, and the fact that they are line-tied at each end. A schematic of the result of wrapping the field lines is given in Figure A6, which shows the two planes to which the footpoint displacements have been applied, along with the resultant distribution of field lines (labelled with arrows). The field line about which all the others wrap is shown as the vertical dashed line. The bold field lines lie wholly in front of the vertical line, while the dotted field lines lie wholly behind both these and the vertical field line. The result of the magnetic tension

and the line-tying forces the field lines to compress on top of one another, producing the strong currents that we see. In particular we note that despite the shear the main component remains that in the z -direction. Hence the single isosurface encompassing the current layer shown in Figure A4. However, the components j_x and j_y retain information relating to the imposed shears, and hence have a change of sign on passing through the current layer in j_z . Therefore, j_x and j_y have local maxima on both sides of the j_z current layer, and this explains the fact that they each reveal isosurfaces either side of this layer.

While the isosurfaces reveal the general structure of the equilibrium current, we have lost a sense of direction in them. This can be recovered by considering some specific contours. In particular, Figure A7 shows contours of j_x in planes of constant z starting from the bottom plane, and working up to the mid-plane. There is no need to go further in z since, as the isosurfaces show, the structures simply continue to rotate from those below the mid-plane, albeit in the opposite direction. The dotted contours are for negative current values. We now clearly see the effect of shear, with j_x reversing direction about a specific line below the mid-plane, and actually reversing about the line $y = 0$ in the mid-plane itself. For j_x , then, the structure in z is tantamount to taking the mid-plane contours and slowly “sliding” them past one another as you descend or ascend through the planes.

The equivalent contours for j_y are shown in Figure A8. The mid-plane contours now reverse across the line $x = 0$. As you move through the planes in z the contours rotate together, unlike the “sliding” observed in j_x . The sets of contours for j_x and j_y not only have a certain spatial symmetry, but also their amplitudes in that in each contour the maximum (positive) contour is always the same magnitude as the minimum (negative) contour. The absolute maxima are (a) 16.4, (b) 9.9, and (c) 5.3 for j_x in Figure A7, and (a) 7.8, (b) 10.2, and (c) 12.0 for j_y in Figure A8. We see that j_x is tending to dominate j_y close to the lower boundary, while the opposite is true by the time we reach the mid-plane.

As we would anticipate from the isosurface plot, the contours of j_z shown in Figures A9(a)-(c) are dominated by the vertical (positive) component. We also recover the sense of a single feature that rigidly rotates as we progress from the lower to the upper boundary. Specifically, the maximum and minimum contour values are (a) 36.5 and -9.9, (b) 37.8 and -

4.6, and (c) 37.5 and -3.5, respectively. These contours also reveal how remarkably uniform the current concentration in j_z is with regard to its length and breadth in each z -plane. We can therefore simply use the dimensions of the current concentration in the mid-plane as a reference point. Furthermore, since we obtain equilibrium solutions, then the current \mathbf{j} must be everywhere parallel to the magnetic field \mathbf{B} . Hence knowing the field line topology immediately gives us the current topology.

As we have indicated, the main aim of these experiments is to determine whether or not current concentrations or sheets are possible in these sheared equilibria. Since the anticipated scalelengths are well below those accessible numerically, it is only through tests of the numerical convergence of our solutions that we can make predictions about the behaviour of the actual coronal fields. It is therefore important to have suitable reference points in each solution that can be reliably measured, so as to allow the checks for convergence. Global checks of the total current are one measure, as well as any local current maxima. Here, the mid-plane solution provides such a useful reference point. In particular, the current concentration associated with j_z is clearly produced by the shortening of the scales in the x direction. We will therefore use the distance across the line $x = 0$ between the two points where the current falls to half its peak value along the line $y = 0$ as a relevant indicator of convergence.

Having defined this half-width length scale, we can map this on to the the number of grid points that an equivalent Eulerian code would require to gain the same resolution as the Lagrangian code. These are shown in Table 1. Obviously one could argue that an Eulerian code could used a number of methods, for example a stretched grid, to gain more resolution. However an equivalent method could normally be applied to the Lagrangian code. For the largest shears we have been able, with the use of the Lagrangian formulation coupled with nonlinear multigrid, to resolve current structures of approximatley 1/1000th the size of the computational domain. This is an order of magnitude better than an equivalent Eulerian code (see for example Galsgaard and Nordlund (1996)). It should be noted, however, that the Lagrangian formulation by definition can only examine ideal MHD, and unlike resistive Eulerian codes nothing can be said about reconnection or subsequent evolution once resistive effects come into play. The resulting high

resolution can however point to whether the current structures seen in resistive codes are indeed “current sheets” or just current concentrations that would allow slow reconnection at solar values of resistivity. Here slow is with regard to observed timescales.

Figure A10 shows a plot of maximum current against half-width (Δ) as the number of grid points is increased. Only the two shears that appear to give a divergent current are shown. A tentative extrapolation may be carried out to the width of a structure allowed by solar resistivity. Fitting a power law to the data in figure A10 gives the relationship $j_m = 3.78/\Delta^{0.81}$. This corresponds, for a lengthscale collapse of about six orders of magnitude, to a current of the order of $3 \times 10^5 B_0/(\mu L_0) \text{ Am}^{-2}$, where B_0 and L_0 are characteristic magnetic field strengths and field line lengths. Taking $B_0 = 10\text{G}$ and $L_0 = 10^6\text{m}$ this gives a current density of $2 \times 10^6 \text{ Am}^{-2}$. If the energy within the current sheet is released by Joule dissipation then this total energy may be calculated as

$$j_D = \int j^2/\sigma dv \quad (5)$$

giving $j_D = 4 \times 10^{18} \text{ J}$. For dissipation by reconnection acting on the Alfvén time scale (say the order of 100 seconds) we would get an energy flux of approximately $4 \times 10^4 \text{ Js}^{-1} \text{ m}^{-2}$ over the area of the box. Given the number of assumptions in making the above calculation, it is still interesting to see that this value is comparable with energy flux observed in active regions of $10^4 \text{ Js}^{-1} \text{ m}^{-2}$ (see for example Withbroe and Noyes (1977)).

A further measure of how close our solutions are to the true equilibrium can be gained by plotting the integral of $|\mathbf{j}|$ over whole the box and the magnetic energy within the box against the resolution used. Both of these quantities should converge with increasing resolution for an equilibrium solution, whether a current sheet is formed or not. We show these plots in Figure A11. It can be seen, in all cases, that there is a smooth convergence with increasing number of grid points.

4. Discussion and Conclusions

In this paper we have addressed the issue of the production of current concentrations or sheets in nonlinear, force-free equilibria in coronal magnetic fields. Previous work suggests that the combination of a

shear plus a shear is sufficient to do so, and we therefore focus on such footpoint displacements. Our results to date show that for certain amplitudes of the second shear, convergent, well-resolved equilibria can be generated. However, beyond a critical point it seems that the equilibria are divergent, in the sense that for increasing numbers of fluid elements we find convergence in the total current and magnetic energy in the system, but that a local current peak (and its associated scalelength) are not convergent. On extrapolating these latter results to scalelengths expected in the coronal environment, we would predict that currents of sufficient magnitude to account for significant heating can be generated. Whether these equilibria are singular in the sense of leading to current sheets we cannot determine. Nevertheless, the current anticipated is sufficiently concentrated to make the point academic; layers of resistively heated plasma will be present.

Furthermore, by use of a Lagrangian approach, we have been able to access scalelengths well below those attained by any Eulerian code to date. The Lagrangian code allows fluid elements to migrate into those regions where scalelengths are reducing, and therefore makes it particularly suitable for such equilibrium experiments. Field lines are also simply plotted by tracing through the positions of the fluid elements; there is no recourse to the use of integration routines etc. One disadvantage of the classical relaxation method is its slow rate of convergence for the most intensive solutions (in terms of complexity and number of grid points). Through the use of nonlinear multigrid methods we have been able to partially overcome this problem. Thus converged solutions to these most important experiments can be calculated in finite times.

If the reader is seeking a black and white answer to whether Parker or van Ballegooijen is correct on the question of the nature of coronal equilibria, then this is not the place to look. There is certainly no degree of symmetry assumed in our simulations; they are fully three-dimensional. Nevertheless our imposed footpoint distributions have a certain symmetry to them. As for the equilibria, we would contend that we find both well resolved, fully three-dimensional solutions, as well as those that demonstrate a level of divergence. This puts us firmly on the fence. Whatever one’s views, we do present compelling evidence for the generation of significant current concentrations in the corona.

The question of the timescale required to produce such structures is an important one. We only see the final product in terms of the relaxed solution once the footpoint displacements have been imposed. It must be left to others to determine whether a fully dynamical corona can do likewise. Nevertheless, as pointed out by Galsgaard and Nordlund (1996), the timescale for the footpoint motions is at least a factor of a hundred less than that of the characteristic Alfvén transit time, and one would therefore expect a significant amount of time for near equilibrium conditions to evolve. Future dynamical experiments with such separation of timescales will have to be performed to demonstrate the truth or otherwise of this assertion.

As ever, we have only begun to scratch the surface. Our bias towards the Lagrangian approach ensures that we will continue to employ such methods time dependently, hopefully to answer some of the questions of timescale. We are also following up the work of van Ballegooijen (1988b) with an Eulerian approach using the Euler potentials. With the advent of nonlinear multigrid methods and more powerful workstations, it seems entirely appropriate to see how far we can push the Eulerian codes in this context!

The authors wish to express their gratitude to Klaus Galsgaard for his prompting on the issue of flux-braiding and to the referee for a number of useful comments.

A. The Implementation of Multigrid

Here we outline our implementation of nonlinear multigrid with respect to the above problem. More detailed accounts of multigrid can be found in Brandt (1977), McCormick (1987) and for M.H.S. relaxation theory Cally (1991), Fiedler (1992), Longbottom, Fiedler and Rickard (1997).

The key to understanding multigrid methods is to know why classical methods fail. Classical relaxation methods are extremely efficient at smoothing out short wavelength errors, those on the scale of the grid spacing. However they are poor at smoothing longer wavelength errors. The trick with multigrid is to restrict the problem on to successively coarser grids, smoothing the errors in each case, and then prolongate the more accurate solution back on to the finer grids. As smoothing on the coarser grids takes significantly less time than smoothing on the finest

grid such a multigrid sweep, smoothing all wavelength errors, is much more efficient than a number of iterations on the finest grid smoothing only short wavelength errors.

We implement a full approximation scheme (F.A.S.) fixed schedule multigrid, including F-cycles. This proceeds as follows:

For solving $F(\mathbf{x}) = \mathbf{j} \times \mathbf{B} = 0$, we start with a first guess for \mathbf{x} (\mathbf{x}_F^n) and (pre) smooth on the fine grid to find the next best estimate \mathbf{x}_F^{n+1} . We then compute the *residual* $\mathbf{r}_F = F(\mathbf{x}_F^{n+1})$, and restrict both \mathbf{x}_F^{n+1} and \mathbf{r}_F to the next coarsest grid by a second order three dimensional weighting $\mathbf{r}_C = \mathcal{R}(\mathbf{r}_F)$ and $\mathbf{x}_C^n = \mathcal{R}(\mathbf{x}_F^{n+1})$. Here \mathcal{R} represents the restriction operator. The approximate solution to the equation $F(\mathbf{x}_C) = \mathbf{r}_C + F(\mathbf{x}_C^n)$, (\mathbf{x}_C^{n+1}) is then calculated on this coarser grid (by recursive multigrid calls to successively coarser grids). We then *prolongate* the correction to the solution, $\mathbf{x}_C^{n+1} - \mathbf{x}_C^n$, back up to the finer grid by trilinear interpolation and add it to the best estimate on the fine grid $\mathbf{x}_F^{n+2} = \mathbf{x}_F^{n+1} + \mathcal{P}(\mathbf{x}_C^{n+1} - \mathbf{x}_C^n)$. Finally a further (post) smooth is carried out using \mathbf{x}_F^{n+2} as the initial guess for the relaxation. This completes one multigrid sweep.

In general the efficiency of the process is dependent on the order in which the coarser grids are visited. We find, for this problem, that an F-cycle is the best choice. Thus for a four leveled system (labeled 1 to 4 from coarse to fine) one multigrid F-cycle visits the grids in the order 4-3-2-1-2-1-2-3-2-1-2-3-4.

Ideally for Multigrid the number of iterations should scale independently from N (the number of points on the finest grid), however in many complex 3D nonlinear cases the scaling is with some power of N that lies between 0 and 2. We find here that the number of iterations scale like N as opposed to N^2 for the classical method.

Figure A12 compares the convergence of the classical and multigrid versions of the ADI relaxation method. The residual force measures the error in the solution over the whole domain. One work unit (WU) is the cpu time for one iteration on the finest grid. The examples shown are for grids of 33^3 and 65^3 points after the second (x -axis) shear of magnitude 0.2 has been applied. In both cases the convergence of the classical method soon saturates (once short wavelength errors have been smoothed), however the multigrid method continues to converge. Also the scalings with number of grid points for both classi-

cal and multigrid methods can be seen.

Lagrangian resolution	Effective Eulerian resolution for given shear:						
	0.8	0.2	0.3	0.4	0.5	0.6	0.7
21^3	26^3	39^3	42^3	46^3	48^3	50^3	52^3
31^3	26^3	46^3	58^3	70^3	82^3	92^3	96^3
33^3*	26^3	47^3	60^3	76^3	85^3	118^3	120^3
41^3	26^3	50^3	68^3	92^3	134^3	200^3	308^3
51^3	27^3	54^3	77^3	96^3	188^3	286^3	556^3
61^3	27^3	58^3	85^3	133^3	234^3	462^3	—
65^3*	27^3	58^3	86^3	136^3	240^3	521^3	943^3

Table 1: The effective number of grid points needed by an Eulerian code to resolve the current structures obtained using the Lagrangian code. Resolutions marked * were calculated using nonlinear multigrid.

REFERENCES

Billinghurst, M. N., Craig, I. J. D., and Sneyd, A. D., 1993 *A&A*, 279, 589

Brandt, A., 1977, *Mathematics of Computation*, 31, 333

Browning, P. K., and Hood, A. W., 1989, *Sol. Phys.*, 124, 271

Cally, P. S., 1991, *J. Chem. Phys.*, 93, 411

Craig, I. J. D., and Sneyd, A. D., 1986, *ApJ*, 311, 451

Craig, I. J. D., and Sneyd, A. D., 1990, *ApJ*, 357, 653

Fiedler, R. A. S., Proc. of the First SOHO Workshop, Annapolis, Maryland, USA, 273

Galsgaard, K. and Nordlund, A., 1996, *J. Geophys. Res.*, 101, A6, 13, 445

Gold, T., 1964, *The Physics of Solar Flares*, 389, W.N. Hess, NASA, SP-50

Hendrix, D. L. and Van Hoven, G., 1996, *ApJ*, 467, 887

Longbottom, A. W., Fiedler, R. A. S. and Rickard, G. J., 1997, *A&ASupp.*, submitted

Longcope, D. W. and Strauss, H. R., 1994a, *ApJ*, 426, 742

Longcope, D. W. and Strauss, H. R., 1994a, *ApJ*, 437, 851

Longcope, D. W. and Sudan, R. N., 1994, *ApJ*, 437, 491

McCormick, S. F., 1987, *Multigrid Methods, Frontiers in Applied Mathematics*, Vol 3, Society for Industrial and Applied Mathematics, Philadelphia, PA

Mikić, Z., Schnack, D. D. and Van Hoven, G., 1989, *ApJ*, 338, 1148

Parker, E. N. R., 1972, *ApJ*, 174, 499

Parker, E. N. R., 1983, *ApJ*, 264, 642

Parker, E. N., 1994, *Spontaneous Current Sheets in Magnetic Fields*, International Series on Astronomy and Astrophysics, OUP

van Ballegooijen, A. A., 1985, *ApJ*, 298, 421

van Ballegooijen, A. A., 1986, *ApJ*, 311, 1001

van Ballegooijen, A. A., 1988a, *Geophys. Ap. Fluid Dynamics*, 41, 181

van Ballegooijen, A. A., 1988b, Proc. 9th Sacramento Peak Summer Workshop on Solar and Stellar Coronal Structure and Dynamics, p. 115

van Ballegooijen, A. A., 1990, Priest, E.R. and Krishan, V., *Basic Plasma Processes on the Sun*, I.A.U., Netherlands, 303

Withbroe, G. L. and Noyes, R. W., 1977, *ARA&A*, 15, 363

Fig. A1.— Footpoint displacements applied on the plane $z = -L_z$. The displacements on the plane $z = +L_z$ are the mirror images of those shown, reflected in the planes $x = 0$ and $y = 0$.

Fig. A2.— Maximum current j_m obtained in the best relaxed solution for each distribution of footpoints, plotted against n_a (see text).

Fig. A3.— Magnetic field structure for the first type of relaxed solution. The magnetic fields shown are (a) B_x , (b) B_y , and (c) B_z .

Fig. A4.— Isosurface of the j_z current component at 50 per cent of the maximum current in the equilibrium solution. The vertical direction is z going between -0.5 and 0.5 . The remaining directions are x and y forming a right-handed set and varying between -0.3 and 0.3 .

Fig. A5.— Isosurfaces of the (a) j_x , and (b) j_y currents at 25 and 42 per cent of the maximum currents for each component, respectively. The cube orientation and dimensions are as the previous Figure.

Fig. A6.— Schematic of field-line wrapping resulting from the application of two shears. The field lines are labelled with an arrow.

Fig. A7.— Contours of the current j_x in the planes (a) $z = -0.5$, (b) $z = -0.25$, and (c) $z = 0$.

Fig. A8.— Contours of the current j_y in the planes (a) $z = -0.5$, (b) $z = -0.25$, and (c) $z = 0$.

Fig. A9.— Contours of the current j_z in the planes (a) $z = -0.5$, (b) $z = -0.25$, and (c) $z = 0$.

Fig. A10.— Maximum current against half-width for a varying number of grid points. Only the two second shears, 0.6 (Δ) and 0.7 (\times) that have diverging currents are shown.

Fig. A11.— The convergence of the total integrated current and magnetic energy as the number of grid points are increased.

Fig. A12.— Residual force against WU for a shear of 0.2 with 32^3 (*) and 64^3 (\times) intervals, respectively. Dashed curves show the classical method, solid curves nonlinear multigrid.

